Onset of the vortexlike Nernst signal above T_c in $La_{2-x}Sr_xCuO_4$ and $Bi_2Sr_{2-y}La_yCuO_6$

Yayu Wang,[1] Z. A. Xu,[1,*] T. Kakeshita,[2] S. Uchida,[2] S. Ono,[3] Yoichi Ando,[3] and N. P. Ong[1]
[1]*Joseph Henry Laboratories of Physics, Princeton University, Princeton, New Jersey 08544*
[2]*School of Frontier Sciences, University of Tokyo, Yayoi 2-11-16, Bunkyo-ku, Tokyo 113-8656, Japan*
[3]*Central Research Institute of Electric Power Industry (CRIEPI), Komae, Tokyo 201-8511, Japan*
(Received 16 August 2001; published 21 November 2001)

The diffusion of vortices down a thermal gradient produces a Josephson signal which is detected as a vortex Nernst effect. In a recent report by Xu *et al.* [Nature **406**, 486 (2000)], an enhanced Nernst signal identified with vortex-like excitations was observed in a series of $La_{2-x}Sr_xCuO_4$ (LSCO) crystals at temperatures 50–100 K above T_c. To pin down the onset temperature T_ν of the vortexlike signal in the lightly doped regime ($0.03 \leqslant x \leqslant 0.07$), we have reanalyzed the carrier contribution to the Nernst signal in detail. By supplementing Nernst measurements with thermopower and Hall-angle data, we isolate the off-diagonal Peltier conductivity α_{xy} and show that its profile provides an objective determination of T_ν. With the results, we revise the phase diagram for the fluctuation regime in LSCO to accommodate the lightly doped regime. In the cuprate $Bi_2Sr_{2-y}La_yCuO_6$, we find that the carrier contribution is virtually negligible for y in the range 0.4–0.6. The evidence of an extended temperature interval with vortexlike excitations is even stronger in this system. Finally, we discuss how T_ν relates to the pseudogap temperature T^* and the implications of strong fluctuations between the pseudogap state and the *d*-wave superconducting state.

DOI: 10.1103/PhysRevB.64.224519 PACS number(s): 74.40.+k, 72.15.Jf, 74.72.−h, 74.25.Fy

I. INTRODUCTION

Close to the the upper critical field line $H_{c2}(T)$ of a type-II superconductor, vortices exist in a ''vortex liquid'' state as highly mobile excitations. In this mobile state, the vortices readily flow in response to a weak applied temperature gradient toward the cooler end of the sample. By the Josephson effect, the vortex motion generates an electric field $\mathbf{E}=\mathbf{B}\times\mathbf{v}$ that lies perpendicular to both the vortex velocity $\mathbf{v}$ and $\mathbf{B}=\mu_0\mathbf{H}$ [Fig. 1(a)]. In general, the appearance of a transverse $\mathbf{E}$ in the presence of a thermal gradient and magnetic field is known as the Nernst effect.[1] In weak fields, the Nernst *signal* $E_y/|\nabla T|$ increases linearly with B, but, at higher fields, the curve of E_y vs T tends to develop negative curvature. The Nernst coefficient ν is defined as the Nernst signal per unit B in the weak-B limit. Because a field-antisymmetric E_y may be measured to high resolution, the Nernst effect provides a highly sensitive probe for detecting vortices.

From the purview of conventional superconductivity, the search for vortices high above the critical temperature T_c seems quite unrewarding. Above T_c, the average value of the condensate density n_s is zero. Although fluctuation effects produce small evanescent droplets of superconductivity detectable by susceptibility and resistivity, the existence of a Nernst signal in the fluctuation regime above T_c is not expected. Indeed, vortex Nernst signals in the fluctuation regime do not seem to have been reported for any low-T_c superconductor. In the first Ettinghausen[1] experiment on a cuprate ($YBa_2Cu_3O_7$), however, Palstra *et al.*[2] noted that the signal extended ~ 10 K above T_c.

Later Nernst experiments on cuprates (restricted to optimally doped samples) found that the vortex signal extends above T_c by roughly the same interval.[3–5] Because the relative temperature interval ~ 0.1 is small, these observations did not provoke much theoretical comment. More recently, Corson *et al.*[6] investigated the conductivity in thin-film $Bi_2Sr_2CaCu_2O_8$ at terahertz frequencies, and found that the kinetic inductance of the superfluid is observed as high as 25 K above T_c.

In Nernst measurements on $La_{2-x}Sr_xCuO_4$ (LSCO), Xu *et al.*[7] observed that the Nernst signal remains anomalously en-

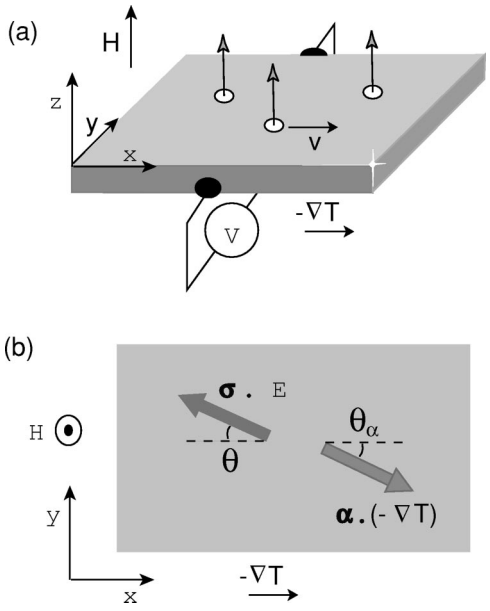

FIG. 1. (a) Geometry of the Nernst experiment in the vortex liquid state. Vortices (disks with vectors) flow with velocity $\mathbf{v}$ down the gradient $-\nabla T\|\hat{\mathbf{x}}$. Phase slippage induces a dc signal E_y that is antisymmetric in H. The lower panel (b) shows the currents $J_i=\sigma_{ij}E_j$ and $J_i'=\alpha_{ij}(-\partial_j T)$ produced by the E field and thermal gradient, respectively, in the normal state. The slight difference between their y components engenders the carrier Nernst signal (angles θ and θ_α are defined in the text).

hanced 50–100 K above T_c, from which they inferred the existence of vortexlike excitations in the putative ''normal state.'' Starting at a relatively small and nearly T-independent value at high temperatures, ν begins to diverge at an onset temperature T_ν, until it peaks near T_c at a value 500–1000 times larger than the value at onset. Because of the specific symmetry properties of the Nernst signal ($\mathbf{E}\|\mathbf{B}\times\nabla T$), Xu *et al.* argued that the excitations are vortexlike. Moreover, they noted that the anomalous signal is very sensitive to Nd doping (which suppresses T_c to $\sim$8 K), and *smoothly evolves to the familiar vortex signal* below T_c. A closely similar extended fluctuation regime was also observed in underdoped $YBa_2Cu_3O_y$.[8]

The important issue of whether the observed excitations correspond to magnetic vortices or are excitations in a strongly correlated state (for, e.g., holes bound to vorticity in an electronic state) is at present open. Indeed, the notion that vortices of whatever origin can be detected 50–100 K *above* T_c remains as surprising and challenging to us (and many in the community) as when they were first observed. Hence, as in Ref. 7, we refer to them generically as *vortexlike* excitations in this paper. We also refer to the region between T_c and T_ν generically as a ''fluctuation'' regime. (A discussion of this issue in relation to the pseudogap state is given in Sec. V.)

Our goal in this paper is to sharpen the distinction between a vortexlike signal from that produced by normal-state charge carriers in order to address several issues raised in Ref. 7 (we also provide extended discussions of many issues that were only touched on there). The onset temperature of the vortex signal T_ν appears to increase with decreasing hole density x. Is T_ν finite in the $x\to 0$ limit? If not, how does T_ν behave in this limit? How significant is the normal-state carrier contribution to ν in the small-x regime? Can a more objective separation of the vortex signal be obtained through a better understanding of the normal-state Nernst effect? Are these excitations seen in other cuprates?

The small-x regime requires a more careful analysis of the carrier Nernst signal because the normal-state thermopower is strongly enhanced. We introduce a new method suitable for this limit, and apply it to $La_{2-x}Sr_xCuO_4$ (LSCO) and the single-layer cuprate $Bi_2Sr_{2-y}La_yCuO_6$ (Bi 2201). We isolate the key quantity in the Nernst experiment—the off-diagonal Peltier current—and show that it provides an objective procedure for separating the vortex signal that is particularly suited for the small-x regime. The results enable us to obtain a revised phase diagram for fluctuations in LSCO that is valid in both the small- and large-x regimes. In Bi 2201, we find that the vortexlike signal, relative to the normal carrier contribution, is even larger than in LSCO. Hence T_ν may be obtained directly from the original Nernst signal without need for isolating the Peltier current.

II. ISOLATING THE PELTIER CURRENT

To explain our procedure, we recall the various charge currents generated in a Nernst experiment (initially we consider the normal-state terms only). We take the thermal gradient $-\nabla T\|\hat{\mathbf{x}}$ and the field $\mathbf{H}\|\hat{\mathbf{z}}$. The Nernst signal is the H-antisymmetric electric field $\mathbf{E}\|\hat{\mathbf{y}}$ per unit gradient (Fig. 1).

In zero field, the applied gradient drives a charge current density $\mathbf{J}=\alpha(-\nabla T)$ along the length of the sample [we define the Peltier conductivity tensor α_{ij} by $J_i=\alpha_{ij}(-\partial_j T)$ and for brevity write $\alpha_{ii}=\alpha$]. To satisfy the boundary condition $J_x=0$, there must exist an $\mathbf{E}$ field to drive a current σE_x in the opposite direction (σ is the electrical conductivity). Hence the total current along $\hat{\mathbf{x}}$ is

$$J_x=\sigma E_x+\alpha(-\partial_x T). \tag{1}$$

With $J_x=0$, we have $E_x=-(\alpha/\sigma)(-\partial_x T)$, which is the signal detected in a thermopower experiment. The thermopower coefficient is $S=\alpha/\sigma$.

In a finite field, the two currents in Eq. (1) spawn Hall-type currents (antisymmetric in H) flowing along the y axis [Fig. 1(b)]. One is the familiar Hall current $\sigma_{yx}E_x$ while the other is the *off-diagonal* Peltier current $\alpha_{yx}(-\partial_x T)$, where σ_{yx} and α_{yx} denote the Hall and off-diagonal Peltier conductivities, respectively. These two off-diagonal currents are opposite in direction and nearly equal in magnitude. (The standard Boltzmann-theory expressions for these currents are given in the Appendix.) Because of the experimental boundary condition $J_y=0$, any residual difference between the off-diagonal currents leads to a weak E_y which is then detected as the Nernst signal. Hence we have

$$\begin{aligned} J_y&=\alpha_{yx}(-\partial_x T)+\sigma_{yx}E_x+\sigma E_y \\ &=\left[\alpha_{yx}-\sigma_{yx}\frac{\alpha}{\sigma}\right](-\partial_x T)+\sigma E_y=0. \end{aligned} \tag{2}$$

We have dropped a term $\alpha(-\partial_y T)$, which is important in conventional metals but negligible in cuprates (see Appendix). Using the Hall angle $\tan\theta=\sigma_{xy}/\sigma$ in Eq. (2), for the Nernst coefficient due to charge carriers alone we obtain

$$\nu_N=\frac{E_y}{|\partial_x T|B}=\left[\frac{\alpha_{xy}}{\sigma}-S\tan\theta\right]\frac{1}{B}. \tag{3}$$

At first glance, it may seem that ν_N is just the thermopower S reduced by the Hall angle $\tan\theta$ (since it derives from a current transverse to the applied gradient). However, by writing Eq. (3) as $\nu=S[\tan\theta_\alpha-\tan\theta]/B$, with $\tan\theta_\alpha\equiv\alpha_{xy}/\alpha$, we see that the reduction factor involves a cancellation between the two angles θ and θ_α [see Fig. 1(b)]. As shown by Sondheimer,[9] within Boltzmann theory the cancellation is exact if θ is independent of energy ϵ (see the Appendix). [Because of this cancellation, the ratio E_y/E_x in a Nernst experiment does not represent a ''Hall angle'' for entropy currents.]

A useful order-of-magnitude estimate of $|\nu_N|$ is $|S\tan\theta/B|$, reduced by a factor of 10 (to account for the Sondheimer cancellation). For LSCO in the range $0.1<x<0.17$, $S\simeq 10\ \mu$V/K and $\tan\theta/B\leq 10^{-2}\ \mathrm{T}^{-1}$, we estimate $|\nu_N|\leq 10$ nV/KT, which is what is generally observed. This rule of thumb anticipates that when S is of the order of 100 μV/K, $|\nu_N|$ may become as large as 50 nV/KT (see below).

Diagonal and off-diagonal response. Even if we disregard the Sondheimer cancellation, the carrier Nernst signal (being

off-diagonal) is ''small'' compared with the (diagonal) thermopower signal whenever $\tan\theta \ll 1$. By contrast, the vortex Nernst signal represents the ''large'' response of the vortices to an applied $-\nabla T$. If the flux-flow Hall angle $\tan\theta_f \ll 1$ (as in the cuprates), the vortex velocity $\mathbf{v}$ is very nearly $\parallel (-\nabla T)$. Hence the Josephson field $\mathbf{E_J}$ represents the diagonal response of the flux motion (even though it appears as a transverse Hall-type signal). On the other hand, the small velocity component $v_y = v_x \tan\theta$ transverse to $-\nabla T$ leads to a signal detected as the flux-flow thermopower S_f, which *is the small off-diagonal signal* in the vortex liquid. This reversal of roles for the Nernst and thermopower signals in going from the normal state to the vortex-liquid state reflects the well-known duality between vortex and charge currents, and is the primary reason why the Nernst experiment is so useful for detecting vortex motion. The vortex Nernst signal reflects the *primary* response of vortices to an applied gradient, while the carrier Nernst effect is a relatively feeble off-diagonal response that is further attenuated by the Sondheimer cancellation.

For our present purpose, we are interested in the temperature range when the diagonal vortex signal has fallen to values comparable with the carrier signal. The contribution of the vortices to the observed Nernst signal may be written as an off-diagonal term α_{xy}^s that adds to the normal-state term α_{xy}^n (now relabeled with n). Repeating the steps above, we find that the combined Nernst signal is comprised of three terms, viz.

$$\nu = \frac{E_y}{|\partial_x T| B} = \left[\frac{\alpha_{xy}^s}{\sigma} + \frac{\alpha_{xy}^n}{\sigma} - S\tan\theta \right] \frac{1}{B}. \tag{4}$$

In Ref. 7, we assumed that the Sondheimer cancellation was sufficiently complete to reduce ν_N below a threshold of ~ 4 nV/KT. Hence any increase of ν above this threshold was identified with the vortex term α_{xy}^s/σ. This ''threshold criterion'' is valid for moderately large x, where $|S|$ is small. However, when $x \ll 1$, another approach is needed. For samples with $x \leqslant 0.07$, the thermopower S (which sets the scale for α_{ij}) rises to values in the range 100–300 μV/K. This strong enhancement means that ν_N may significantly exceed the threshold, the Sondheimer cancellation notwithstanding.

Our method is based on measuring S and $\tan\theta$ separately at each T. By subtracting the product $-S\tan\theta$ from ν in Eq. (4), we obtain the total off-diagonal Peltier term

$$\left[\frac{\alpha_{xy}}{\sigma} \right]_{obs} = \frac{\alpha_{xy}^s}{\sigma} + \frac{\alpha_{xy}^n}{\sigma}. \tag{5}$$

An important point is that α_{xy}^n must decrease to zero as $T \to 0$ because it is a carrier-entropy current, just like α (the same is true of ν_N). By contrast, the vortexlike contribution α_{xy}^s strongly diverges as $T \to T_c$ from above, as the phase stiffness of the superconducting condensate increases. If T_c is very small (as in $L2$), the vortex term appears as a divergent signal as T decreases. This is a key point in what follows.

III. EXPERIMENTAL RESULTS

The Nernst experiments are carried out in a thermal gradient (4 K/cm below 50 K and 8 K/cm above) applied along $\hat{\mathbf{x}}$. The temperature difference ΔT between the sample ends (measured with chromel-alumel thermocouples) is ~ 0.5 K below ~ 50 K and ~ 1 K above (the crystals are all cut to a length between 1.0 and 1.5 mm). The Nernst voltage E_y is measured with a nanovoltmeter (Keithley 2001 with preamp 1801) while the field is slowly ramped at a rate of 0.4 T/min between -8 and 8 T (or ± 14 T in high-resolution runs). Prior to ramping H, we regulate T to a stability of ± 1 mK (this takes 30 min). The drift of the voltmeter in zero H (~ 10 nV over a 1-h period) is sufficiently small to guarantee a reproducibility in the Nernst coefficient of ± 1 nV/KT (about four times higher in resolution than attained in Ref. 7).

The need to measure nV signals reproducibly in a temperature gradient introduces specific experimental constraints for single crystals. The present method of sweeping the field (in both directions) at *fixed* temperature is quite necessary to attain accuracies better than 100 nV/KT. The alternative, faster, method of sweeping T in a fixed field (with a repeat in reversed field) is error prone and unreliable even if T is swept at the rate of 1 K/min. The reason is apparently the very long relaxation time of the temperature gradient within the crystal. In our experience, such constant-H traces versus T, though useful for a qualitative overview of ν, are of limited accuracy.

A. LSCO

With the higher resolution, we have remeasured ν in a series of LSCO samples [$L1$, $L2$, $L3$, $L4$, and $L5$ with x (T_c) = 0.03 (0 K), 0.05 (<4 K), 0.07 (12 K), 0.12 (28.9 K), and 0.20 (32.5 K), respectively] (S and $\tan\theta$ were also measured in $L1$–$L3$, but not in $L4$ and $L5$). The variation of the Nernst signal $E_y/|\nabla T|$ with H displayed in Fig. 2 (for sample $L4$) is quite representative of LSCO. At 20 K, for instance, E_y rises steeply from zero when H exceeds the melting field $H_m \simeq 2$ T, approaching saturation at values 6–7 μV/K at high fields.

On warming across T_c ($=28.9$ K), the overall magnitude of the signal decreases (as does H_m). Remarkably, instead of dropping to zero, the Nernst signal remains large as T rises to 60 K, high above T_c. We note that a negative curvature is present even at 40 K. This would not be expected from the normal-state Nernst signal in a system with such short carrier lifetimes. From such curves, ν is determined from the initial slope at each selected T. The T dependence of ν is displayed in Fig. 3 for the three most underdoped LSCO samples. [For later discussion (Sec. V), we note that ν continues to increase up to 14 T in the curves at 27 and 30 K.]

As previously reported,[7] ν in sample $L3$ ($x = 0.07$) is very small and nearly T independent (-5 to -10 nV/KT between 300 and 130 K). Below ~ 130 K, it begins an inexorable increase that ultimately reaches 2 μV/KT at 12 K. Using the threshold method, we previously identified 130 K as

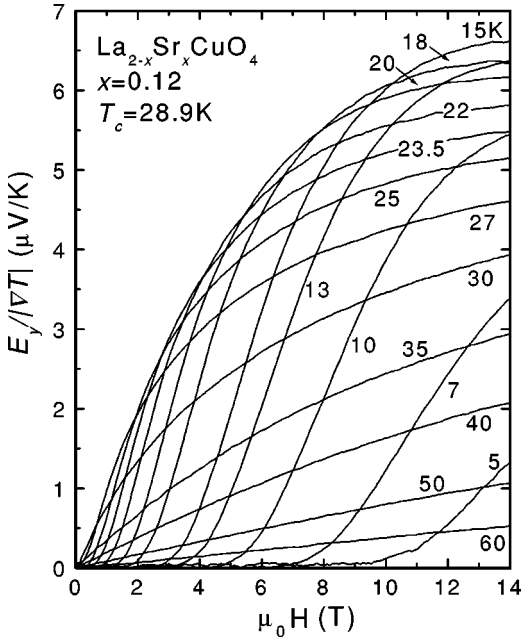

FIG. 2. The field dependence of the Nernst signal $E_y/|\nabla T|$ in $La_{2-x}Sr_xCuO_4$ (sample $L4$, $x=0.12$) at fixed T from 5 to 60 K. E_y rises steeply when H exceeds H_m (~ 5 T at 10 K). For T just below T_c ($=$ 28.9 K), $H_m \simeq 0$, and E_y vs H shows a very pronounced negative curvature. The curves continue to display curvature up to 50 K. Note the relatively slow decay of the signal at 14 T above T_c.

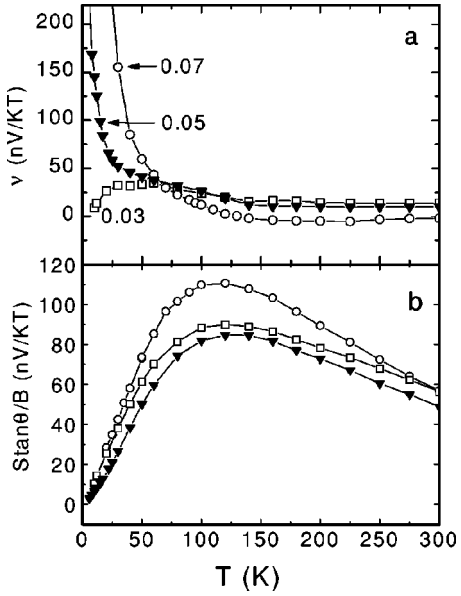

FIG. 3. (a) The T dependence of ν in very underdoped LSCO (samples $L1$, $L2$, and $L3$, with $x=0.03$, 0.05 and 0.07, respectively). At low T, the different behaviors of ν in $L1$ (compared with $L2$ and $L3$) indicate distinct origins of the Nernst signal. In $L1$ (open squares), ν is entirely from the carriers, while in $L2$ and $L3$, is from vortexlike excitations. The lower panel (b) displays $S\tan\theta/B$ measured in $L1$–$L3$ [symbol associations are the same as in (a)]. Above 150 K, cancellation is nearly complete between the two normal-state currents, $S\tan\theta/B$ and α^n_{xy}. At lower T, however, a significant residual ν_N is observed, especially in $L1$.

the onset temperature. However, a gradual increase starting near 130 K is also apparent in both samples $L2$ ($x=0.05$) and $L1$ ($x=0.03$). In $L2$, ν continues to increase at lower T. Significantly, however, in the sample with the lowest doping $L1$, ν attains a broad peak and then *decreases* toward zero. As discussed above, the latter behavior is characteristic of ν_N.

In very underdoped samples, the thermopower is so large ($S\sim 300$ μV/K at 100 K in $L1$) that the maximum value of ν_N (40 nV/KT) greatly exceeds the 4-nV/KT threshold. The juxtaposition of the last two curves shows especially clearly that the threshold method should be supplanted with another technique more appropriate for samples with very large S.

Using the measured thermopower and Hall angle, we have obtained the curves $S\tan\theta$ displayed in Fig. 3(a) for $L1$–$L3$. The two panels in Fig. 3 illustrate the Sondheimer cancellation at temperatures above 150 K. In $L3$ ($x=0.07$), $|\nu|$ is ~ 10 nV/KT at 150 K whereas $S\tan\theta/B \simeq 110$ nV/KT. Hence both the normal-state off-diagonal currents $S\tan\theta$ and α^n_{xy}/σ must be closely matched in magnitude [see Eq. (3)]. This cancellation is much less effective at low T, especially in $L1$.

Subtracting $S\tan\theta/B$ from ν, we obtain the Peltier curves $\alpha_{xy}/\sigma B$ shown in Fig. 4. In $L1$, $\alpha_{xy}/\sigma B$ (open squares) rises to a broad maximum near 100 K before falling toward zero as $T\rightarrow 0$. This behavior, characteristic of normal carriers, allows us to identify α_{xy} with α^n_{xy} at all T in $L1$. Sample $L2$ displays a closely similar profile (solid triangles) except that, below 50 K, the decrease is interrupted by the onset of the vortex term at 40 K (arrow).

Hence, removal of the contribution $S\tan\theta$ has made the onset of the vortex term quite unambiguous. Our results show that even at $x=0.05$, fluctuation effects arising from pair formation are observed starting at 40 K. In $L3$, the onset of the vortexlike term at 90 K may also be identified by the inflection point (arrow). To estimate the vortex contribution α^s_{xy}/σ in $L2$ and $L3$, we assume their normal contribution α^n_{xy}/σ has nearly the same form as $\alpha_{xy}/\sigma B$ in $L1$ apart from a slight re-scaling [as suggested by the similarities in the profiles of $S\tan\theta/B$ in Fig. 3(b)]. In $L2$, we believe this procedure is quite reliable, since the total α_{xy} is so closely matched to that in $L1$ above 40 K (and α^n_{xy} must approach zero as $T\rightarrow 0$). In $L3$, the assumption is less objective. However, errors incurred (of magnitude ± 10 nV/KT) are relatively insignificant because α^s_{xy}/σ rapidly inflates to values 1–2 μV/KT.

The steep increase in the vortex-like contributions in $L2$ and $L3$, displayed as the shaded regions in Fig. 4, is rather striking. In $L2$, we note that the anomalous signal starts near 40 K even though T_c is nominally zero (below 4 K). These plots represent one of our key findings.

B. Bi 2201

The systematic variation of transport properties and hole concentration with La content y in single-layer Bi 2201 was been investigated by Ando *et al.*[10] With increasing hole den-

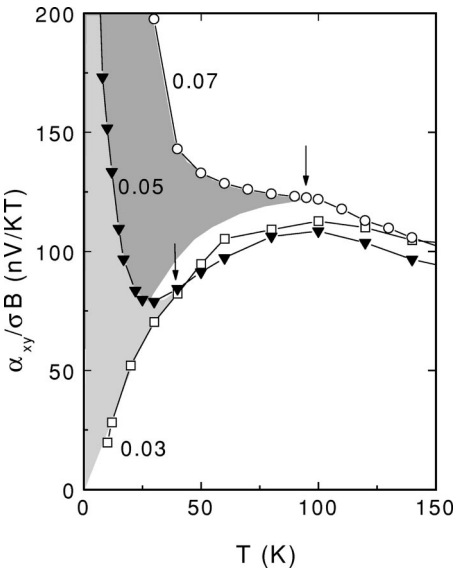

FIG. 4. The T dependence of the Peltier off-diagonal term α_{xy} in $L1$–$L3$ obtained by subtracting $-S\tan\theta/B$ from ν [see Eq. (4)]. In $L1$ ($x=0.03$), the profile of α_{xy} (decreasing to zero as $T\rightarrow 0$, open squares) identifies it as arising entirely from the carriers. In $L2$ ($x=0.05$) and $L3$ ($x=0.07$), however, the onset of the vortex term α_{xy}^{s} is apparent as an inflection point (arrows). The shaded regions are estimates of the vortexlike term $\alpha_{xy}^{s}/\sigma B$ in $L2$ and $L3$. Note that, at sufficiently low T [below the melting line $H_m(T)$], the vortex Nernst signal must vanish as the vortices become a solid (not shown).

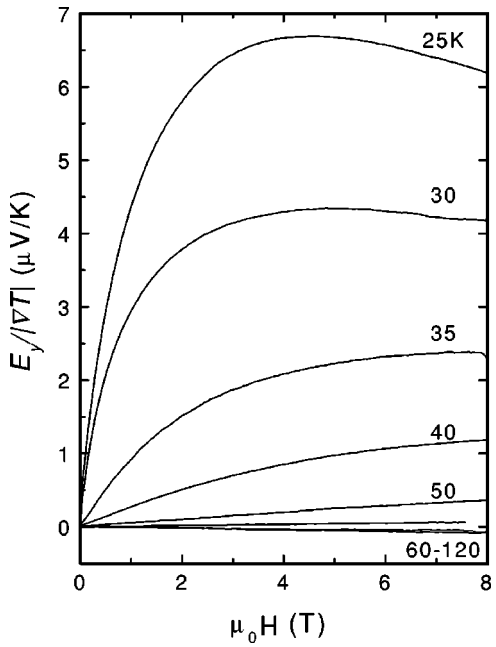

FIG. 5. Variation of $E_y/|\nabla T|$ vs H in $Bi_2Sr_{2-y}La_yCuO_6$ (sample $B2$ with $y=0.5$) at temperatures 25–120 K. Compared with LSCO, the curves display more pronounced curvatures at temperatures high above T_c.

sity (decreasing y), T_c goes through the familiar dome-shaped curve, attaining its maximum value ~ 35 K at $y=0.4$.[11]

We have investigated three samples $B1$, $B2$, and $B3$ in which y (T_c) $=0.6$ (17 K), 0.5 (29 K), and 0.4 (32 K), respectively. Magnetization measurements show a relatively sharp Meissner transition at T_c, and the virtual absence of diamagnetic screening above (see below). The field dependence of the Nernst signal in $B2$ (Fig. 5) is representative of the three Bi 2201 samples. Below T_c, the trace of E_y vs H displays a highly pronounced curvature. In comparison with LSCO, the negative curvature persists to higher temperatures above T_c. As the hole mean free path (MFP) is very short (see below), it is clear that the curvature cannot arise from the normal-state contribution ν_N. Rather, the strong sensitivity to these moderate fields is consistent with a superconducting fluctuation origin.

The values of ν measured in a field of 1 T are displayed in Fig. 6. The gradual decrease of ν over an extended range of T above T_c bears a striking resemblance to the profiles in LSCO (see Fig. 2 of Xu *et al.*[7]). The values of T_ν are also quite similar.

We have also measured S and $\tan\theta$ in $B1$ and $B2$ (but not in $B3$). In contrast to very underdoped LSCO, $S\tan\theta/B$ is generally quite small in these samples. As seen in Figs. 7 and 8, the largest values attained by $S\tan\theta/B$, 10 and 6 nV/KT in $B1$ and $B2$, respectively, are an order of magnitude smaller than in samples $L1$–$L3$. Most of the suppression comes from the shorter MFP (as determined from $\tan\theta$) in Bi 2201, which leads to greatly reduced normal-state off-diagonal currents $S\tan\theta$ and α_{xy}^{n}.

Applying the new method to $B1$ and $B2$, we now find that the curves of $\alpha_{xy}/\sigma B$ and ν differ only slightly (by ~ 10 nV/KT in the range 70–150 K) (Figs. 7 and 8). Thus there is little difference (given the measurement uncertain-

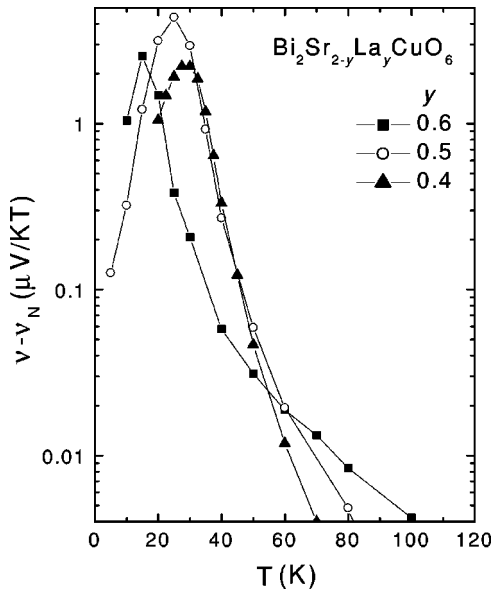

FIG. 6. The T dependence of ν in Bi 2201 (samples $B1$, $B2$, and $B3$ with $y=0.6$, 0.5, and 0.4, respectively). At all T, we determined ν from the values of $E_y/|\nabla T|$ observed at 1 Tesla (this slightly underestimates ν when curvature is pronounced near T_c; see Fig. 5). T_ν decreases systematically as the hole concentration increases (from $B1$ to $B3$).

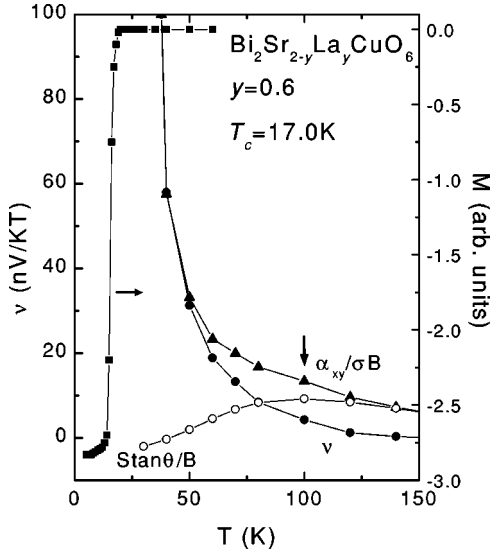

FIG. 7. The T dependence of ν (solid circles), $S\tan\theta/B$ (open circles) measured in sample $B1$. The Peltier term $\alpha_{xy}/\sigma B$ (solid triangles) is obtained as the sum of these two curves (all refer to left scale). T_ν is estimated from ν using the threshold criterion (vertical arrow) (ν_N is less than 2 nV/KT up to 300 K). The magnetization curve (from the zero-field-cooling curve measured in a 10 Oe field) shows a sharp Meissner transition at $T_c \simeq 17$ K (solid squares).

ties) whether we use ν or $\alpha_{xy}/\sigma B$ to estimate T_ν (this could not have been anticipated, however, without isolating α_{xy}). The strongly suppressed $S\tan\theta$ provides very strong *quantitative* arguments against identifying the increase in ν below T_ν with the normal state carriers. [From Fig. 8, the observed α_{xy} in $B2$ increases by ~ 50 nV/KT between 80 and 50 K. It would be difficult to imagine a scenario in which this increase comes from the hole carriers when $S\tan\theta$ is actually decreasing from 6 to ~ 3 nV/KT over the same temperature range.]

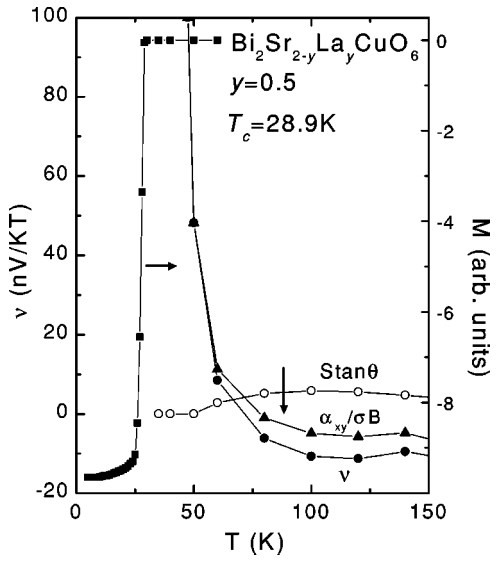

FIG. 8. The T dependence of ν (solid circles), $S\tan\theta/B$ (open triangles), and $\alpha_{xy}/\sigma B$ (solid triangles) in sample $B2$ (left scale). As in Fig. 7, T_ν is indicated by the arrow (ν_N is ~ -10 nV/KT up to 300 K). The magnetization curve shows a sharp Meissner transition at $T_c \simeq 29$ K (solid squares).

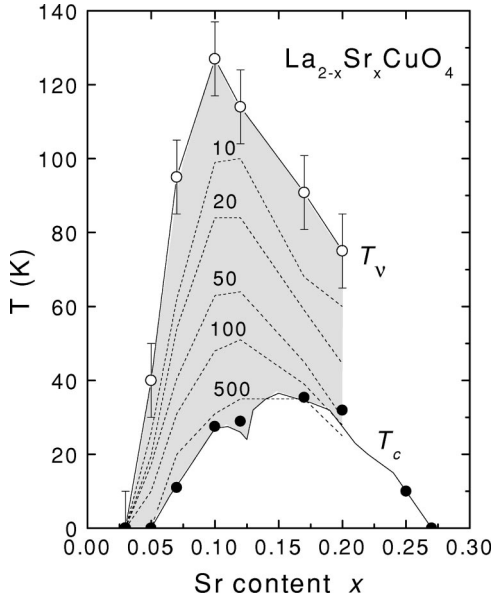

FIG. 9. The x dependence of T_ν and the contours of the vortex-like Nernst signal in LSCO. For the very underdoped samples $L1$–$L3$, T_ν is determined from α_{xy} as explained in the text. For $L1$–$L3$, the numbers by the contour lines refer to the magnitude of $\alpha^s_{xy}/\sigma B$ derived from Fig. 4. For samples with $x>0.07$, we have used the procedure of Xu *et al.* (Ref. 7) to determine T_ν (the contour values are then the magnitudes of $\nu-\nu_N$). Data for the two samples with $x=0.10$ and 0.17 are taken from Xu *et al.*

In addition, as mentioned above, the Nernst signal E_y vs H develops increasingly pronounced negative curvature below 50 K. Curvature in fields less than 8 T cannot arise from hole carriers with such short lifetimes. We find these arguments supporting vortexlike excitations in the range T_c to ~ 80 K especially compelling in Bi 2201. In Figs. 7 and 8, we have also displayed the relatively sharp Meissner transition determined from the diamagnetic susceptibility in $B1$ and $B2$, respectively. The comparison emphasizes that in the large interval between T_ν and T_c, ν rapidly diverges, but the Meisnner response is essentially non-observable.

IV. PHASE DIAGRAM OF FLUCTUATIONS

With the results in samples $L1$–$L3$, we have revised our previous phase diagram for LSCO.[7] Figure 9 shows the values of T_ν together with the contours of α^s_{xy}/σ estimated in samples $L2$ and $L3$ (shaded regions in Fig. 4). For samples at higher doping ($x \geqslant 0.10$), we display contours corresponding to values of $\nu-\nu_N$, since, as explained above, our procedure is unnecessary if $x>0.07$.

In the revised diagram, vortexlike excitations are absent at all T in the sample with $x=0.03$. Between 0.03 and 0.07, T_ν increases very steeply from 0 to 90 K with a slope dT_ν/dx of at least 2400 K (the slope is larger if $T_\nu \simeq 0$ at $x=0.04$ as well). T_ν peaks at ~ 128 K at $x=0.10$, and then decreases

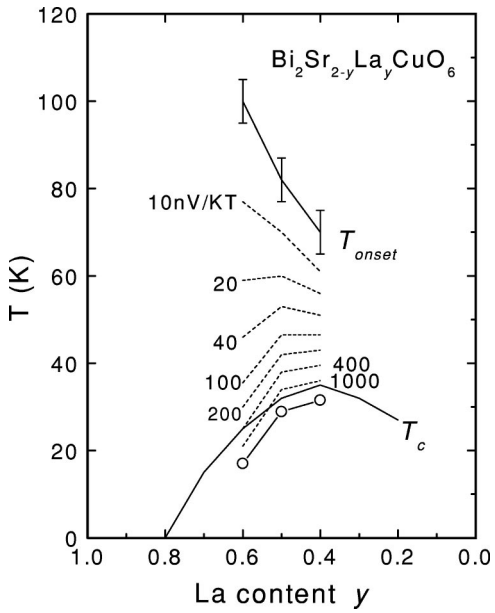

FIG. 10. The y dependence of T_ν and the contours of the vortexlike Nernst signal in $Bi_2Sr_{2-y}La_yCuO_6$. The numbers next to the contours refer to the magnitude of $\nu-\nu_N$ determined by the procedure of Xu *et al.* (Ref. 7). The solid line for T_c is from Ono *et al.* (Ref. 11) (open circles are T_c measured in $B1-B3$). The contours bear a strong resemblance to those in LSCO (Fig. 9).

nearly linearly with x, but at the slower rate ($dT_\nu/dx \sim -510$ K).

We have also plotted T_ν and the contours of the anomalous Nernst signal $\nu-\nu_N$ for $B1$, $B2$, and $B3$ in the phase diagram of Bi 2201 (Fig. 10). T_ν decreases with increasing hole content (decreasing y), as observed in LSCO for $x > 0.12$. The scale of T_ν is similar to that in LSCO (as is T_c).

The phase diagrams in these single-layer cuprates brings out several interesting features. The fluctuation regime extends to a maximum temperature 100–130 K that is considerably higher than the maximum T_c in either cuprate. In this large interval, vortexlike excitations are readily detected, but no Meissner signal appears until T_c is reached. The contrast is especially dramatic in $B1$ and $B2$ (Figs. 7 and 8).

The onset temperature has a different dependence on doping than T_c. Instead of mimicking the shape of T_c vs x, T_ν peaks at 0.10 in LSCO. Hence the fluctuation regime is noticeably skewed toward the underdoped side (it also extends more deeply into the small-x region than the superconducting phase). We note that the skewedness is evident in all the contours up to 100 nV/KT in Fig. 9, not just in T_ν. It is intriguing that in strained films of LSCO,[12] which display a $\sim$20% improvement in T_c compared to bulk samples, the T_c vs x curve shows also a similar skewedness (the contour at 50 nV/KT in Fig. 9 matches well the T_c curve in the strained films[12]). In Bi 2201, the less complete data set also shows that the fluctuation regime extends to higher T at lower hole concentration (larger y). The asymmetry suggests that the strength of the fluctuation regime, as measured by the magnitude of $\nu-\nu_N$, tends to increase monotonically with decreasing x (until it suddenly collapses when x is too small). The peaking of T_ν at $x=0.10$ in LSCO is interesting because it is close to the $x=\frac{1}{8}$ state, where spin-density-wave fluctuations (or stripe fluctuations) appear to be strongest. Our inclination, however, is to interpret the peaking of T_ν as simply reflecting the sharp interruption (near 0.1) of the rising trend of T_ν with decreasing x, but these interesting trends deserve further study.

This general trend suggests that the energy scale associated with pair formation is largest at small x, falling nearly linearly as x increases. Because of strong fluctuations, long-range phase coherence—necessary to sustain a Meissner effect—occurs at a T_c that is much lower than T_ν.

V. PSEUDOGAP AND STRONG FLUCTUATIONS

A key point of interest is the relation of the vortex-like excitations to the pseudogap state.[13,14] In LSCO, information on T^* is largely derived from heat capacity. The shoulder in $\gamma(T)=c_e(T)/T$ (where c_e is the electroinc heat capacity) provides the estimate that T^* is equal to $\sim$350 K at $x=0.08$, and decreases linearly to $\sim$90 K at $x=0.22$.[14,15] However, there appears to be a lack of corroboration for the estimated T^* from nuclear magnetic resonance (NMR) relaxation, infrared reflectivity, in-plane resistivity ρ, or tunneling. The NMR relaxation rate $1/T_1T$ does not show the broad maximum that is a key signature of the pseudogap, while ρ does not display the shoulder seen in other underdoped cuprates.

In Bi 2201, Fischer's group recently reported that the gap in the density of states observed by scanning-probe tunneling spectroscopy[16] is observed up to $\sim$68 K (but the sharp ''coherence'' peaks at the gap maxima collapse at $T_c \simeq 11$ K). The c-axis resistivity profile, however, suggests a much higher T^* (100, 125, and 250 K for La contents $y=0.4$, 0.5, and 0.6, respectively).[17]

The available evidence implies that T_ν is roughly a factor of 2 lower than T^* in LSCO and Bi 2201 (or much closer, if we use the tunneling data in Bi 2201). With the improved resolution for T_ν achieved here, the uncertainties now lie chiefly in T^*. [We note, however, that estimates of T^* in any cuprate vary considerably, depending on the particular experimental probe used.[13] The differences may arise from the highly anisotropic nature of the pseudogap magnitude and the fact that a particular experimental technique is sensitive to excitations at a particular wave vector $\mathbf{q}$.]

With these caveats stated, we note that the contours in Figs. 9 and 10 are consistent with the x dependence of T^* (away from the lightly doped regime). This suggests that the energy scale for destroying the vortex excitations depends on x in the same way as T^*. This trend, suggestive of strong pairing tendencies in the lightly doped regime, recalls early theories of cuprate superconductivity,[18] which proposed that, in the single-layer parent material, pairing correlations are already ''built in'' in the spin-$\frac{1}{2}$ antiferromagnet.

Fluctuation regime. The physical picture suggested is that the pseudogap state, while distinct from d-wave superconductivity, is nevertheless closely similar in important aspects. Pairing correlations seem to be already intrinsic at high temperatures in the pseudogap state, and fluctuations between the two states become ever stronger as we cool away from

T^*. Even at temperatures 50–100 K above T_c, these pairing correlations begin to support vortexlike excitations that are detectable as an anomalous Nernst signal. Closer to T_c (within 10–20 K), the phase-rigidity length inflates dramatically to reach macroscopic length scales. This increase is reflected in the rapid growth of ν as reported by Xu *et al.*[7] (the concomitant increase in kinetic inductance also becomes observable at Terahertz frequencies[6] in this interval). In the conventional picture of strong phase fluctuations, the case for an extended fluctuation regime above T_c was made by several theorists.[20,21] In theories of strongly interacting systems, a discussion of fluctuations between the pseudogap state and *d*-wave superconductivity in the SU(2) theory was recently published by Lee and Wen.[22]

Perhaps the most interesting question raised by these experiments is whether the vortex-like excitations are the familiar vortices in a superconducting condensate or electronic excitations specific to the pseudogap state. Is it possible that, closer to T_ν, the excitations are more properly regarded as vortexlike defects of the pseudogap state rather than Abrikosov vortices? We elaborate further on two points mentioned above. The first is the *continuity* between the anomalous Nernst signal above T_c and that in the Abrikosov state below. If we view the Nernst signal $E_y/|\nabla T|$ as a function of both H and T, it is apparent that the fluctuation regime covers a very wide region in the H-T plane. In this paper, we have traced the large fluctuating regime as we move along the T axis in zero field. The fluctuation regime uncovered is actually part of a very large region of the H-T plane (as may be seen by scanning H at fixed T). As noted in the curves in Fig. 2, the vortex Nernst signal at temperatures near T_c continues to increase with H (up to 14 T) . We do not observe a decrease of the Nernst signal that might flag the crossing of an "H_{c2}" line regardless of how close we get to T_c. A detailed analysis of the low-T data shows that the high-temperature fluctuation regime connects continuously with the high-field fluctuation regime below T_c (the extended phase diagram of the fluctuations will be reported elsewhere). By the continuity argument, the vortexlike excitations—if distinct—must evolve smoothly into Abrikosov vortices as T decreases towards T_c.

The interesting counterpoint is that the onset of the Meissner response is relatively sharp (Figs. 7 and 8). The resistivity profile also implies that conventional amplitude fluctuations in the sense of Aslamasov and Larkin[19] occur in a fairly narrow interval. Unlike in conventional superconductors, the diagmagnetic response and resistivity do not "see" the large fluctuation regime uncovered by the Nernst signal above T_c. These two experimental points are seemingly at odds from the viewpoint of conventional theories of fluctuations, but we believe they provide very important hints. Resurgent interest in this interesting regime seems likely, and we may expect the Nernst effect to play a key role in elucidating its properties (for, e.g., its sensitivity to Zn and its extension into the overdoped regime).

Summary. We have applied the Nernst effect to investigate vortex motion at elevated temperatures in crystals of $La_{2-x}Sr_xCuO_4$ and $Bi_2Sr_{2-y}La_yCuO_6$. To address the lightly doped regime specifically, we have adopted an experimental procedure to sharpen the difference between the vortexlike Nernst signal and the carrier Nernst signal near the former's onset temperature T_ν. The total Nernst signal is comprised of a term in the off-diagonal Peltier current α_{xy} and a term involving the Hall angle $S\tan\theta$. Combining measurements of the latter with the Nernst effect, we may back out the α_{xy} current. We show that in LSCO samples with $x \leqslant 0.07$ (in which S is very large), the profile of $\alpha_{xy}/\sigma B$ very clearly shows the onset of vortexlike terms (arrows in Fig. 4). Our analysis allows the phase diagram in LSCO to be revised to accommodate the lightly doped regime. The fluctuation regime (which harbors these vortexlike excitations) is observed to extend to a maximum temperature of 130 K and to be skewed toward the underdoped side. Applying the same procedure to three samples of La-doped Bi 2201, we show that the carrier contribution to ν is essentially negligible. Its (partial) phase diagram shares many similar features with that of LSCO. We emphasize the deep penetration of the vortexlike regime into the pseudogap state, and interpret the results in terms of strong fluctuations between the pseudogap state and the *d*-wave superconducting state. We discuss whether the vortexlike excitations are identical with vortices of the superconducting condensate or interesting electronic excitations of the pseudogap state.

ACKNOWLEDGMENTS

The research at Princeton was supported by the U.S. National Science Foundation (MRSEC Grant No. NSF-DMR 98-09483). N.P.O. and S. U. acknowledge support from a grant from the New Energy and Industrial Tech. Develop. Org., Japan (NEDO). We wish to thank P. W. Anderson, J. Clayhold, S. Kivelson, P. A. Lee, A. J. Millis, V. N. Muthukumar, J. Orenstein, and Z. Weng for helpful dicussions.

APPENDIX: CARRIER NERNST COEFFICIENT IN BOLTZMANN APPROACH

Here we summarize the standard expressions for the Nernst coefficient in conventional metals. Carriers diffusing in a thermal gradient $-\nabla T$ in the presence of $\mathbf{E}$ and a weak field $\mathbf{B}$ satisfy the Boltzmann equation

$$\mathbf{v_k}\cdot\frac{\partial f^0}{\partial\epsilon}\frac{(\epsilon_\mathbf{k}-\mu)}{T}(-\nabla T)+\frac{e\mathbf{E}}{\hbar}\cdot\mathbf{v_k}\frac{\partial f^0}{\partial\epsilon}+\frac{e\mathbf{v_k}\times\mathbf{B}}{\hbar}\cdot\frac{\partial f_\mathbf{k}}{\partial\mathbf{k}} = -\frac{g_\mathbf{k}}{\tau_\mathbf{k}}, \tag{A1}$$

where $g_\mathbf{k}=f_\mathbf{k}-f^0_\mathbf{k}$ is the difference between the perturbed distribution function $f_\mathbf{k}$ and its value $f^0_\mathbf{k}$ at equilibrium ($\mathbf{v_k}$ and $\tau_\mathbf{k}$ are the velocity and lifetime in state $\mathbf{k}$). To find the Peltier conductivity elements, we may set $\mathbf{E}=0$, and expand $g_\mathbf{k}=g^{(0)}_\mathbf{k}+g^{(1)}_\mathbf{k}+\cdots$, where $g^{(0)}$ (linear in $-\nabla T$) gives α while $g^{(1)}$ (linear in $-\nabla T$ and B) gives the off-diagonal term α_{xy}. By iteration of Eq. (A1), we have

$$g^{(0)}_\mathbf{k}=-\tau_\mathbf{k}\frac{\partial f^0}{\partial\epsilon}\mathbf{v_k}\cdot\frac{(\epsilon_\mathbf{k}-\mu)}{T}(-\nabla T), \tag{A2}$$

$$g_{\mathbf{k}}^{(1)}=\frac{e\mathbf{v}_{\mathbf{k}}\times\mathbf{B}}{\hbar}\cdot\frac{\partial g_{\mathbf{k}}^{(0)}}{\partial\mathbf{k}}. \tag{A3}$$

The off-diagonal current J_y is just $eg^{(1)}\mathbf{v}_{\mathbf{k}}$ integrated over the Fermi surface. Hence the off-diagonal conductivity is [in terms of the mean-free-path $\vec{l}(\mathbf{k})\equiv\mathbf{v}_{\mathbf{k}}\tau_{\mathbf{k}}$] is

$$\alpha_{yx}=e^2\sum_{\mathbf{k}}\frac{(\epsilon_{\mathbf{k}}-\mu)}{T}\left(-\frac{\partial f^0}{\partial\epsilon}\right)l_y\frac{\mathbf{v}_{\mathbf{k}}\times\mathbf{B}}{\hbar}\cdot\frac{\partial l_x}{\partial\mathbf{k}}. \tag{A4}$$

In two-dimensional systems [with an arbitrary dependence of $l(\mathbf{k})$ on $\mathbf{k}$], we may use the swept-area representation[23] to reduce this complicated expression to

$$\alpha_{xy}=\frac{2e^2B}{(2\pi)^2T\hbar^2}\int d\epsilon\left(-\frac{\partial f^0}{\partial\epsilon}\right)(\epsilon-\mu)\mathcal{A}_l(\epsilon), \tag{A5}$$

where $\mathcal{A}_l(\epsilon)=\oint dl_x l_y$ is the area swept out by $\vec{l}(\mathbf{k})$ as $\mathbf{k}$ goes around a contour at energy ϵ. As σ_{xy} is proportional to $\mathcal{A}_l(\mu)$,[23] we find

$$\alpha_{xy}=\frac{\pi^2}{3}\frac{k_B^2T}{e}\left[\frac{\partial\sigma_{xy}}{\partial\epsilon}\right]_\mu. \tag{A6}$$

This recalls the familiar relation between α and σ:

$$\alpha=\frac{\pi^2}{3}\frac{k_B^2T}{e}\left[\frac{\partial\sigma}{\partial\epsilon}\right]_\mu. \tag{A7}$$

Substituting Eqs. (A4) and (A7) into Eq. (3), and using the small Hall-angle approximation ($\sigma_{xy}/\sigma\simeq\theta$), we have

$$\nu_N=\left[\frac{\alpha_{xy}}{\sigma}-\frac{\sigma_{xy}}{\sigma}\frac{\alpha}{\sigma}\right]\frac{1}{B}=\frac{\pi^2}{3}\frac{k_B^2T}{e}\frac{\theta}{B}\left[\frac{\partial\ln\theta}{\partial\epsilon}\right]_\mu. \tag{A8}$$

If θ is only weakly dependent on energy at ϵ_F (a good approximation in conventional metals), we have a nearly exact cancellation of the two contributions and ν_N is very small.[9]

To estimate ν_N in case $\theta(\epsilon)$ has an anomalously strong power-law dependence ϵ^p, we write $\nu_N\simeq(86\ \mu\text{V/K})[k_BT/\epsilon_F](\theta/B)p$. Using the values $\epsilon_F\sim0.5$ eV, and $(\theta/B)\simeq4\times10^{-3}$ at 100 K (to approximate optimum-doped LSCO), we find that $\nu_N\simeq6p$ nV/KT, which is still small.

Isothermal versus adiabatic conditions. In Nernst experiments on metals in which the electronic thermal conductivity κ^e dominates the phonon conductivity κ^{ph}, the (electronic) thermal Hall conductivity κ_{xy} generates a transverse gradient $-\partial_yT$. This leads to a transverse current comparable to the other transverse currents in Eq. (2), which now reads

$$\begin{aligned}J_y&=\alpha_{yx}(-\partial_xT)+\sigma_{yx}E_x+\alpha(-\partial_yT)+\sigma E_y\\&=\left[\alpha_{yx}-\sigma_{yx}\frac{\alpha}{\sigma}\right](-\partial_xT)+\alpha(-\partial_yT)+\sigma E_y=0.\end{aligned} \tag{A9}$$

Under adiabatic conditions (the transverse edges are free to "float" to different temperatures), we have $-\partial_yT=(\partial_xT)\kappa_{yx}/[\kappa^{ph}+\kappa^e]$. Assuming $\kappa^e\gg\kappa^{ph}$, and writing $\kappa_{yx}/\kappa^e\equiv\eta\sigma_{yx}/\sigma$, where η is a positive number of order 1, we get the equation

$$\left[\alpha_{yx}-(1+\eta)\sigma_{yx}\frac{\alpha}{\sigma}\right](-\partial_xT)+\sigma E_y=0. \tag{A10}$$

Physically, the transverse thermal gradient produces a current that augments the Hall current $\sigma_{yx}E_x$.

Technically, under adiabatic conditions the measured E_y does not give the Nernst coefficient. Heroic efforts are required to "short out" the transverse gradient (for example, by thermally anchoring the transverse edges to each other with a piece of thick wire). Fortunately, in the cuprates, the phonon conductivity κ_{ph} is more than ten times larger than κ^e. Hence the phonons act as a shorting fluid that keeps ∂_yT negligibly small. Measurements of κ_{xy} in YBCO were reported by Zhang *et al.*[24] In LSCO, κ_{xy} is much smaller, and barely detectable.[25] The standard geometry in Fig. 1 is effectively in the isothermal limit for conductors in which $\kappa^e\ll\kappa^{ph}$.

*Present address of ZAX. Department of Physics, Zhejiang University, Hangzhou 310027, China.

[1] See, e.g., Y. B. Kim and M. J. Stephen, in *Superconductivity*, edited by R. D. Parks (Dekker, New York, 1969), Vol. 2, p. 1107.

[2] T. T. M. Palstra, B. Batlogg, L. F. Schneemeyer, and J. V. Waszczak, Phys. Rev. Lett. **64**, 3090 (1990).

[3] S. J. Hagen, C. J. Lobb, R. L. Greene, M. G. Forrester, and J. Talvacchio, Phys. Rev. B **42**, 6777 (1990).

[4] H. C. Ri, R. Gross, F. Gollnik, A. Beck, R. P. Huebener, P. Wagner, and H. Adrian, Phys. Rev. B **50**, 3312 (1994); M. Zeh, H. C. Ri, F. Kober, R. P. Huebener, A. V. Ustinov, J. Mannhart, R. Gross, and A. Gupta, Phys. Rev. Lett. **64**, 3195 (1990).

[5] J. A. Clayhold, A. W. Linnen, F. Chen, and C. W. Chu, Phys. Rev. B **50**, 4252 (1994); J. Clayhold, *ibid.* **54**, 6103 (1996).

[6] J. Corson, R. Mallozzi, J. Orenstein, J. N. Eckstein, and I. Bozovic, Nature (London) **398**, 221 (1999).

[7] Z. A. Xu, N. P. Ong, Y. Wang, T. Kageshita, and S. Uchida, Nature (London) **406**, 486 (2000).

[8] Yayu Wang, Z. A. Xu, N. P. Ong and S. Uchida (unpublished).

[9] E. H. Sondheimer, Proc. R. Soc. London, Ser. A **193**, 484 (1948).

[10] Y. Ando, Y. Hanaki, S. Ono, T. Murayama, K. Segawa, N. Miyamoto, and Seiki Komiya, Phys. Rev. B **61**, R14956 (2000).

[11] S. Ono, Y. Ando, T. Murayama, F. F. Balakirev, J. B. Betts, and G. S. Boebinger, Phys. Rev. Lett. **85**, 638 (2000).

[12] H. Sato, A. Tsukada, M. Naito, and A. Matsuda, Phys. Rev. B **61**, 12 447 (2000).

[13] For a review, see T. Timusk and B. Statt, Rep. Prog. Phys. **62**, 61 (1999).

[14] J. L. Tallon and J. W. Loram, Physica C **349**, 53 (2001).

[15] J. W. Loram, K. A. Mirza, J. R. Cooper, N. Athanassopoulou, and W. Y. Liang, in *Proceedings of the 10th HTS Anniversary Workshop on Physics, Materials and Applications*, edited by B. Batlogg, C. W. Chu, W. K. Chu, D. U. Gubser, and K. A. Muller

(World Scientific, Singapore, 1996), p. 341.
[16] M. Kugler, Ø. Fischer, C. Renner, S. Ono, and Y. Ando, Phys. Rev. Lett. **86**, 4911 (2001).
[17] A. N. Lavrov, Yoichi Ando, and S. Ono (unpublished).
[18] P. W. Anderson, Science **235**, 1196 (1987).
[19] L. G. Aslamazov and A. I. Larkin, Fiz. Tverd. Tela **10**, 1104 (1968) [Sov. Phys. Solid State **10**, 875 (1968)].
[20] V. J. Emery and S. A. Kivelson, Nature (London) **374**, 434 (1995).
[21] M. R. Norman, M. Randeria, H. Ding, and J. C. Campuzano, Phys. Rev. B **57**, 11 093 (1998).
[22] Patrick A. Lee and Xiao-Gang Wen, Phys. Rev. B **63**, 224517 (2001).
[23] N. P. Ong, Phys. Rev. B **43**, 193 (1991).
[24] Y. Zhang, N. P. Ong, Z. A. Xu, K. Krishana, R. Gagnon, and L. Taillefer, Phys. Rev. Lett. **84**, 2219 (2000); Y. Zhang, N. P. Ong, P. W. Anderson, D. A. Bonn, R. Liang, and W. N. Hardy, *ibid.* **86**, 890 (2001).
[25] K. Krishana and N. P. Ong (unpublished).